# Evaluation of Ce-doped $Pr_2CuO_4$ for potential application as a cathode material for solid oxide fuel cells

# Evaluation of Ce-doped $Pr_2CuO_4$ for potential application as a cathode material for solid oxide fuel cells

**L.M. Kolchina[a], N.V. Lyskov[b], A.N. Kuznetsov[a,c], S.M. Kazakov[a], M.Z. Galin[b], A. Meledin[d], A.M. Abakumov[e], S.I. Bredikhin[f], G.N. Mazo[a]*, E.V. Antipov[a]**

## Abstract

$Pr_{2-x}Ce_xCuO_4$ (x = 0.05; 0.1; 0.15) samples were synthesized and systematically characterized towards application as a cathode material for solid oxide fuel cells (SOFCs). High-temperature electrical conductivity, thermal expansion, and electrocatalytic activity in oxygen reduction reaction (ORR) were examined. Electrical conductivity of $Pr_{2-x}Ce_xCuO_4$ oxides demonstrates semiconducting behavior up to 900 °C. Small Ce-doping (2.5 at. %) allows to increase electrical conductivity from 100 to 130 $S \cdot cm^{-1}$ in air at 500-800 °C. DFT calculations revealed that density of states directly below the Fermi level, comprised mainly of Cu 3*d* and O 2*p* states, is significantly affected by atoms in rare earth positions, which might give an indication of a correlation between calculated electronic structures and measured conducting properties. Ce-doping in $Pr_{2-x}Ce_xCuO_4$ slightly increases TEC from $11.9 \cdot 10^{-6}$ $K^{-1}$ for x = 0 to $14.2 \cdot 10^{-6}$ $K^{-1}$ for x = 0.15. Substitution of 2.5 % of Pr atom in $Pr_2CuO_4$ by Ce is effective to enhance electrochemical performance of the material as a SOFC cathode in ORR (ASR of $Pr_{1.95}Ce_{0.05}CuO_4$ electrode applied on $Ce_{0.9}Gd_{0.1}O_{1.95}$ electrolyte is 0.39 $\Omega \cdot cm^2$ at 750°C in air). Peak power density achieved for the electrolyte-supported fuel cell with the $Pr_{1.95}Ce_{0.05}CuO_4$ cathode is 150 $mW \cdot cm^{-2}$ at 800 °C.

## Introduction

High efficiency, fuel flexibility, and low emissions have provoked the great interest in solid oxide fuel cells (SOFCs) development during the last decades[1]. The SOFC characteristics are considered as favorable for stationary power generators. One of the major obstacles that needs to be overcome before successful implementation of SOFCs technology is a poor cathode performance at intermediate temperature (IT) of 500-800 °C[2,3]. Therefore, a good catalyst of oxygen reduction reaction (ORR) is required. It is necessary to keep in mind that cathode performance and long term stability are the result of a multitude of factors such as electronic and ionic conductivity, oxygen exchange kinetics on the surface, and compatibility with a solid electrolyte, thus, an optimal balance between the factors should be kept[4,5]. Nowadays, Co-based oxides such as $La_{1-x}Sr_xCo_{1-y}Fe_yO_{3-\delta}$ (LSCF) and $Ba_{1-x}Sr_xCo_{1-y}Fe_yO_{3-\delta}$ (BSCF) are still state-of-art cathode materials for IT SOFCs despite the existing shortcomings with mechanical stresses and

high degradability under heating-cooling cycling due to high thermal expansion[6,7]. That stipulates an interest in Co-free materials. Another problem, which arises for alkali-earth-containing cathode materials during long operating time, is carbonization. In spite of substantial efforts to lower degradation rate and improve resistance to $CO_2$ at intermediate temperatures, alkali-earth-free materials are still considered preferable[8].

Previously, cuprates with perovskite-related structure have been considered as promising candidates for SOFC application[9-12]. Intense interest in this group of oxides is due to the possible formation and transformation of different crystal structures by a change in the copper coordination from 4- to 6-fold coordinated atoms[13,14]. For example, $Ln_2CuO_4$ (Ln = rare-earth elements) with layered structures crystallize in three different structure types depending on cations in the Ln position[12] . Generally, they demonstrate acceptable thermal expansion behavior (TEC for $Pr_2CuO_4$ = $11.9 \cdot 10^{-6}$ $K^{-1}$, for $Ce_{0.9}Gd_{0.1}O_{1.95}$ = $12.5 \cdot 10^{6}$ $K^{-1}$)[15,16] and their electrical conductivity reaches values ~ $10^2$ $S \cdot cm^{-1}$ and can be enhanced via appropriate doping, that provides effective charge transport[17,18]. A combination of these properties generates interest in studying physical and chemical properties of these oxides at elevated temperature. Moreover, prior studies[19-21] have revealed high electrocatalytic activity in ORR for the rare-earth cuprates.

During the last years one may notice the revived interest in the compounds, which have already been studied mainly as superconductors[22]. The perceptible instance is $Pr_{2-x}Ce_xCuO_4$ phases, which have been known for a long time, with practically only their low-temperature properties having been under scrutiny[23,24]. Their high-temperature properties to the best of our knowledge appeared to be poorly studied. These phases crystallize with T' structure type, which can be presented as an alternation of $Ln_2O_2$ fluorite type slabs and $CuO_2$ sheets along the *c* axis. The Ce-doping in $Pr_2CuO_4$ is expected to have positive influence on conductivity and electrocatalytic properties, enhancing the number of electron charge carriers that can be expressed by the following equation:

$$CuO + 2CeO_2 \xrightarrow{Pr_2CuO_4} Cu_{Cu}^{\times} + 2Ce_{Pr}^{\bullet} + 4O_O^{\times} + 2e' + \tfrac{1}{2}O_2 \qquad (1)$$

Despite that high-temperature conductivity has been mentioned in our previous studies[25], no discussion was made. Also Ce-doped cathode material should demonstrate higher chemical resistivity to GDC electrolyte due to reduction in gradient of Ce concentration, though a good chemical compatibility with GDC electrolyte has already been exhibited by $Pr_2CuO_4$[15]. According to this background, $Pr_{2-x}Ce_xCuO_4$ series deserve to be considered as promising candidates for a SOFC cathode.

In this work, high-temperature electrical conductivity, thermal expansion and electrochemical activity in ORR of $Pr_{2-x}Ce_xCuO_4$ (x = 0.05; 0.1; 0.15) are investigated in order to evaluate their applicability as SOFC cathode materials.

## Experimental

### *Sample preparation and characterization*

$Pr_{2-x}Ce_xCuO_4$ (x = 0; 0.05; 0.1; 0.15) were prepared by a conventional solid-state route from pre-fired $Pr_6O_{11}$, $CeO_2$, and CuO (Sigma-Aldrich®, 99.9%). Appropriate amount of these initial reagents were mixed by a ball-milling under heptane. After drying for 12 hours samples were pressed into pellet and annealed on $Al_2O_3$ crucibles at 1100 ºC for 24 h in air. Oxygen content was determined by iodometric titration. High-temperature X-ray powder diffraction (HT XRPD) data were collected using Bruker D8-Advance diffractometer ($CuK_{\alpha 1}$ radiation, LynxEye PSD) in reflection mode equipped with high-temperature camera XRK-900 (Anton Paar) in air. Unit cell parameters were refined by Rietveld method using TOPAS-3 program package at 298-1073K. Scanning electron microscopy studies were carried out using LEO Supra 50VP. The selected area electron diffraction (SAED) and energy dispersive X-ray spectroscopy (EDX) were performed using Philips CM20 and FEI Tecnai G2 transmission electron microscopes operated at 200 kV. Thermogravimetric analysis (TG) studies was performed in artificial air (20% $O_2$(g), 80% Ar(g)) from 100 to 950 ºC with a heating rate of 10 º/min by Netzsch STA 449C thermoanalyser.

### *Electrochemical studies*

For the DC conductivity measurements single-phase powders prepared by solid-state route were pressed into pellets under pressure of 5 tons per $cm^2$ and sintered at 1000 ºC for 10 h in air. Relative density of the samples determined by a hydrostatic weighing was found to be 80-85 %. Pt-paste was used to create current collectors and potential electrodes on the pellets. Electrical conductivity measurements were performed by conventional four-point DC technique in the temperature range of 100–900 ºC in air using a P-30 potentiostat/galvanostat (Elins Ltd, Russia) in cyclic voltamperometry (CVA) mode in the voltage range from −50 mV to 50 mV at the voltage scan rate of 10 mV/s. To estimate electrochemical performance of electrode materials, the electrochemical cells of an electrode/electrolyte/electrode configuration were fabricated by screen-printing of electrode inks on GDC electrolyte pellets (relative density ~95%) using VS-Monoprint PES HT PW 77/55 (Verseidag-Tecfab GmbH) woven mesh. The electrode inks consisted of $Pr_{2-x}Ce_xCuO_4$ prepared by solid-state route and an organic binder (Heraeus V006), which were taken in the 1:1 ratio. The pellets were then calcinated at 950 °C for 4 h in air. The result electrode thickness was ~ 20 μm. Pt-paste was placed on the face site of GDC pellet then it was annealed at 900 °C for 4 h in air and used as a reference electrode. Electrochemical measurements were carried out by AC impedance spectroscopy using a Z-500P

impedance spectrometer (Elins Ltd, Russia) over the frequency range of 500 MHz to 0.01 Hz at signal amplitude of 30 mV. Measurements were performed using a three-electrode technique at the OCV conditions as a function of temperature (550–800°C) in air.

***Computational details***

Electronic structures of the $Pr_{2-x}Ce_xCuO_4$ compounds with 0, 2.5, 5, and 10 at. % Ce were calculated on the density-functional theory (DFT) level utilizing the all-electron full-potential linearized augmented plane wave method for the band structure calculations as implemented in the ELK code[26], with relativistic effects, including spin-orbit coupling, taken into account. In order to model statistical partial substitution of Pr by Ce, we have employed a virtual crystal approximation (VCA), for which we constructed 'fractional atoms' emulating Pr atoms with the numbers of electrons and atomic masses corresponding to 2.5, 5, and 10% Ce for Pr substitutions. In all cases the Brillouin zone sampling was performed using 195 irreducible k-points. The convergence of the total energy with respect to the k-point sets was checked.

The PBESol exchange-correlation functional[27] of the GGA-type was used in the calculations. The muffin-tin sphere radii for the respective atoms are (Bohr): 2.20 (Pr, Ce), 2.00 (Cu), 1.60 (O). The maximum moduli for the reciprocal vectors $k_{max}$ were chosen so that $R_{MT}k_{max}=8.0$. The convergence criteria for the procedure were set as RMS change in Kohn-Sham potential $< 10^{-5}$ eV, absolute change in total energy $< 10^{-4}$ eV. In order to account for highly localized nature of the 4f electrons of rare earth elements, poorly reproduced by the conventional L(S)DA- and GGA-type exchange-correlation functionals, DFT+U method[28] within the fully localized limit[29] was employed. The values of U and of J for rare earth 4f states were chosen as 7 eV and 0.8 eV according to the literature data[30].

***Fuel cell fabrication and characterization***

An electrolyte-supported fuel cell was fabricated to measure electrochemical performance of $Pr_{2-x}Ce_xCuO_4$ cathodes. For this purpose the 89 mol. % $ZrO_2$ – 10 mol. % $Sc_2O_3$ – 1 mol. % $Y_2O_3$ (10Sc1YSZ) powder (Daiichi Kigenso Kagaku Kogyo Co., Japan) was pressed into a pellet (thickness of 0.50 mm, 20 mm in diameter) and sintered at 1500 °C to form a gas-tight electrolyte membrane (density ~98%). A bi-layer NiO–10Sc1CeSZ (89 mol. % $ZrO_2$ – 10 mol. % $Sc_2O_3$ – 1 mol. % $CeO_2$ (Daiichi Kigenso Kagaku Kogyo Co., Japan)) cermet deposited on one electrolyte side functioned as an anode. To prepare a bi-layered anode the 60 wt. % 10Sc1CeSZ – 40 wt. % NiO and 40 wt. % 10Sc1CeSZ – 60 wt. % NiO pastes were used; they were deposited by turns on one side of the electrolyte, sintered and annealed at 1400 °C in air with additional step at 500 °C for decomposition of the organic binder. The internal and top layers are supposed

to function as a catalyst and current collector, respectively. To prevent chemical reaction between the 10Sc1YSZ electrolyte and the $Pr_{2-x}Ce_xCuO_4$ cathode material a ~5 μm GDC interlayer was coated onto the cathode side of the electrolyte substrate using screen printing, followed by a co-sintering at 1300 °C for 4 hours. A Pt mesh was used as a current collector on the cathode side. To evaluate the $Pr_{2-x}Ce_xCuO_4$ cathode performance under fuel cell operation condition, the composition that exhibited the best characteristics during the primary tests was used. The preparation of this compound was carried out by a freeze-drying technique to obtain the fine powder. For this purpose, pre-fired $Pr_6O_{11}$, CuO and $Ce_2(C_2O_4)_3 \cdot 6H_2O$ with 99.99% purity were dissolved in nitric acid (high purity) in stoichiometric ratio, then polyvinyl alcohol was mixed in 1:5 mass ratio for the stabilization of homogeneous cation distribution. The obtained solution was sprayed into liquid nitrogen. The salt product was first dehydrated by sublimation in "Usifroid SNH-15" freeze-dryer and then calcinated at 800 $^oC$ in air. The cathode ink for single fuel cell test was prepared by mixing of the obtained freeze-drying powder and an organic binder (Heraeus V006), which were taken in the 1:1 ratio. Finally, cathode inks were screen printed to form electrode with area approx. 2 $cm^2$ and sintered at 950°C for 4 hours. The single cell performance was tested using an Autolab 302N potentiostat/galvanostat with humidified $H_2$ as fuel, and synthetic air as an oxidant.

**Results and discussion**

***Powder synthesis and characterization***

X-ray powder diffraction (XRPD) analysis showed the successful synthesis of phase-pure $Pr_{2-x}Ce_xCuO_4$ series with x = 0.05; 0.1; 0.15 (Fig. SI1). The diffraction peaks from all samples were indexed based on the tetragonal crystal structure with space group *I*4/*mmm*. The unit cell parameters for $Pr_{2-x}Ce_xCuO_4$ are in a good agreement with previous studies[31] (Table SI1).

The oxygen content in $Pr_{2-x}Ce_xCuO_{4\pm\delta}$, determined from the iodometric titration, was found to be 4.02(2), 4.01(2), 4.03(2), and 4.05(2) for x = 0, 0.05, 0.10 and 0.15, respectively. A barely measureable oxygen loss ($\delta$ ~ 0.01-0.02) occurs in air between 25 and 900 °C for all studied compounds (Fig. SI2), which agrees with the previously obtained data. A prolonged heating under a reductive atmosphere is required for significant change in oxygen content[31-33]. Thus all studied samples in equilibrium with a gas phase (air) feature oxygen excess at elevated temperatures. To estimate and explain the role of oxygen excess in the n-doped cuprates in charge transport processes many attempts were made, which led to the inference that oxygen excess is conducive for the reduction of charge carrier mobility[34-36]. As a result, both changes in oxygen content and Ce concentration correlate with the number of mobile charge carriers[24]. In case of $Pr_{2-x}Ce_xCuO_{4\pm\delta}$ we can assume that the influence of the oxygen excess can have the

opposite effect on electron charge carrier concentration as compared to change in the dopant content.

Reactivity of $Pr_{2-x}Ce_xCuO_4$ towards GDC solid electrolyte was assessed after annealing of the former powders mixture at 900 $^oC$ for 25 h in air. No additional peaks indicating new phase formation were detected on the XRPD patterns presented in Fig. SI1. Therefore, $Pr_{2-x}Ce_xCuO_4$ can be employed along with GDC electrolyte.

***Electron diffraction study***

Fig. 1 shows selected area electron diffraction (SAED) images for the $Pr_{1.95}Ce_{0.05}CuO_4$ sample. In general, no deviations from the T' crystal structure were found (Fig. 1a). However, some crystallites demonstrating superlattice reflections were accidentally found in the $Pr_{1.95}Ce_{0.05}CuO_4$ sample (Fig. 1b). Similar structural modulations along the [110]/[1-10] directions were previously observed in $Nd_{2-x}Ce_xCuO_4$ and were associated with a twinning and a tetragonal-monoclinic transition[37]. The last one was attributed to the presence of interstitial oxygen atoms. It is worth to note that the number of crystallites displaying superstructure was too low to be considered representative for the bulk of the sample and, presumably, hardly had any substantial impact on the overall sample properties. EDX analysis confirmed the chemical compositions of the all studied samples. In the case of other $Pr_{2-x}Ce_xCuO_4$ samples with $x > 0.05$ no superlattice reflections were observed.

***Thermal expansion behavior***

To study a thermal expansion behavior of $Pr_{2-x}Ce_xCuO_4$, XRPD measurements as a function of temperature were carried out. Fig. 2 shows the linear variation of the unit cell parameters calculated from the HT XRPD as a function of temperature.

Thermal expansion coefficients (TECs) along the *a* and *c* axes, determined using the $V^{1/3}$ vs. T dependencies within the temperature range of 100-800ºC, are summarized in Table 1. As can be seen from the presented data, TECs along the *c* axis gradually increase (up to 57%) as the substitution rate of Ce for Pr is raised. Though the unambiguous reason for such significant increase of TEC is not clear, one can speculate on it. In the case of the $Pr_{2-x}Ce_xCuO_4$, the partial reduction of $Ce^{4+}$ (r = 1.11 Å) to $Ce^{3+}$ (r = 1.28 Å) is possible, though, as was mentioned above, oxygen content may just slightly varies with temperature. At the same time the small substitution of Ce for Pr leads to a slight increase in TEC along the *a* axis.

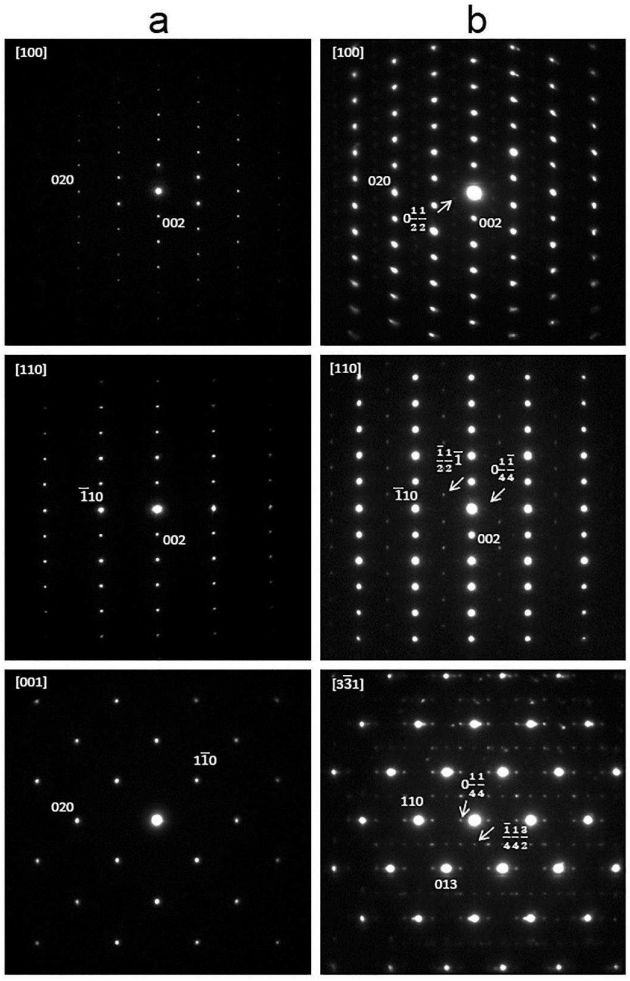


Fig. 1. SAED patterns without (column a) and with (column b) additional ordering of [100], [110], [001] and [331] zones of the $Pr_{1.95}Ce_{0.05}CuO_4$ sample.

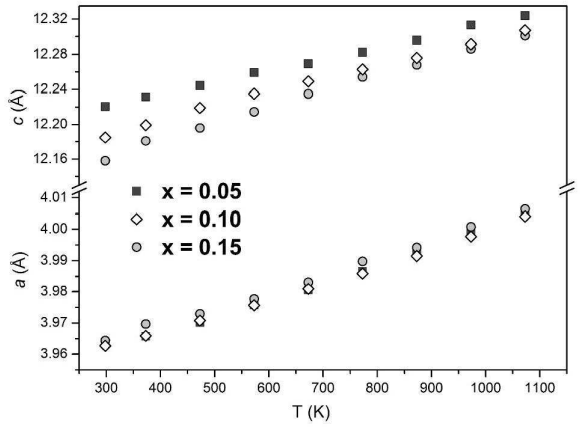


Fig. 2. Unit cell parameters of the $Pr_{2-x}Ce_xCuO_4$ (x = 0.05; 0.1; 0.15) series as a function of temperature.

Table 1

TECs of the $Pr_{2-x}Ce_xCuO_4$ (x = 0.05; 0.1; 0.15) series.

| Compound | $(TEC \pm 0.2) \cdot 10^6$, $K^{-1}$ | | |
|---|---|---|---|
| | $V^{1/3}$ | Along the *a* axis | Along the *c* axis |
| $Pr_2CuO_4$[15] | 11.9 | 13.0 | 9.5 |
| $Pr_{1.95}Ce_{0.05}CuO_4$ | 13.0 | 13.9 | 10.9 |
| $Pr_{1.90}Ce_{0.10}CuO_4$ | 13.3 | 13.5 | 12.7 |
| $Pr_{1.85}Ce_{0.15}CuO_4$ | 14.2 | 13.4 | 14.9 |

Despite the increase in thermal expansion of $Pr_{2-x}Ce_xCuO_4$ with increasing Ce content, the TECs remain acceptable to avoid large mechanical stresses, such as cracking and delaminating during the use of the cuprates as cathode materials with the common solid electrolytes such as $Ce_{0.9}Gd_{0.1}O_{1.95}$.

***Electrical conductivity***

The high electronic conductivity of >100 $S \cdot cm^{-1}$ is preferable for a SOFC electrode to provide a good performance[38]. The Arrhenius plots of electrical conductivity (σ) for the $Pr_{2-x}Ce_xCuO_4$ (x = 0-0.15) phases as a function of temperature within the range of 100-900°C are depicted in Fig. 3.

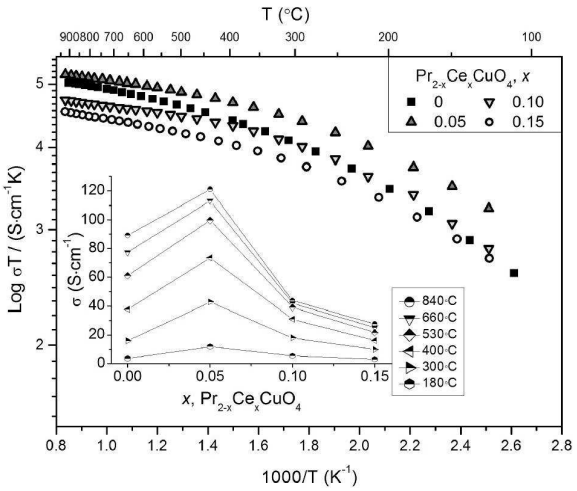


Fig. 3. Dependencies of log σT vs. $10^3/T$ for the $Pr_{2-x}Ce_xCuO_4$ (inset: electrical conductivity of $Pr_{2-x}Ce_xCuO_4$ as a function of Ce-content at different temperatures).

The dependencies show thermoactivation behavior at low temperature of 100-300 °C and in the high temperature range of 450-900 °C. The temperature rise leads to the decrease in the graph slope, which implies a decrease in activation energy. The linear parts can be satisfactory fitted by Arrhenius-like law: $\sigma(T) = \frac{A}{T}\exp(-\frac{E_a}{kT})$, where T is the absolute temperature, $k$ – the Boltzmann's constant, $A$ - a pre-exponential factor, $E_a$ - activation energy. The calculated activation energy for the Ce-doped samples varies in the range of 0.30-0.28 eV at 100-300 °C. These $E_a$ values correspond to activation barrier determined for small polaron hopping mechanism[39]. However, $E_a$ appeared to be two times lower at high temperature, notably, 0.11-0.14 eV at 450-900 °C. The substitution of Ce for Pr slightly reduces the value of the activation barrier: $E_a$ is a bit higher for the undoped $Pr_2CuO_4$ (0.32 eV and 0.17 eV) in the same temperature ranges.

The expected behavior for the $Pr_{2-x}Ce_xCuO_4$ system was an increasing conductivity as Ce content increases due to an electron doping (eq. (1)). Electrical conductivity as a function of the dopant concentration is plotted in Fig. 3 (inset). One may note that the expected behavior is observed for x = 0.05 only. The conductivity for this composition is 1.3-4 times higher in comparison to that for the undoped sample depending on temperature and reaches 100-130 $S \cdot cm^{-1}$ at the IT-SOFC operating temperature, which is desirable for the cathode material. However, a gradual decrease in conductivity occurs as the Ce content is raised. Conductivity drops down for x = 0.10 at temperature above 400°C and for x = 0.15 in comparison to the undoped sample over the studied temperature range. This behavior can be explained by a decrease in concentration of charge carriers due to the presence of extra oxygen atoms in the crystal structure of the $Pr_{2-x}Ce_xCuO_4$:

$$O_i'' + 2Ce_{Pr}^{\bullet} \Leftrightarrow \frac{1}{2}O_2(g) + 2Ce_{Pr}^{x} \qquad (2)$$

Moreover, one must keep in mind that a change in composition of $Pr_{2-x}Ce_xCuO_4$ can provoke considerable modification of the electronic structure. To get more insight into the compositional dependence of electronic structure, DFT calculations for $Pr_{2-x}Ce_xCuO_4$ (x = 0.05, 0.10 and 0.15) were carried out.

***Electronic structure***

In order to investigate the effect of cerium for praseodymium substitutions on the electronic structure of the cuprates in question, we have modeled such substitutions using the virtual crystal approximation and observed the changes in the densities of states (DOS) near the Fermi level (see Fig. 4).

According to our calculations, non-substituted $Pr_2CuO_4$ has rather low yet non-zero density of states at the Fermi level. It is comprised of O 2p- and Cu 3d-states that are strongly hybridized and almost filled (Fig. 3), which means that the band structure calculations predict this compound to exhibit weak metallic properties. It must be noted that the rare earth metal cuprates lie on the metal - charge transfer insulator border[40] and accurate predictions of the conducting properties within the DFT method are highly problematic. Apparently[24,30,41,42], the conductivity of the compounds must be extremely sensitive towards the changes in the copper and oxygen atomic content and environment, which agrees well with what we observe in our calculations. The essential feature of $Pr_2CuO_4$ and other cuprates of this type is the formation of the $CuO_2$ layers, where the strong hybridization of copper and oxygen orbitals is responsible for conductivity of the compounds[41]. Electronic structure of $Pr_2CuO_4$ has not been reported in the literature, but the compound itself has been shown to have the highest conductivity among the rare earth cuprates[24].

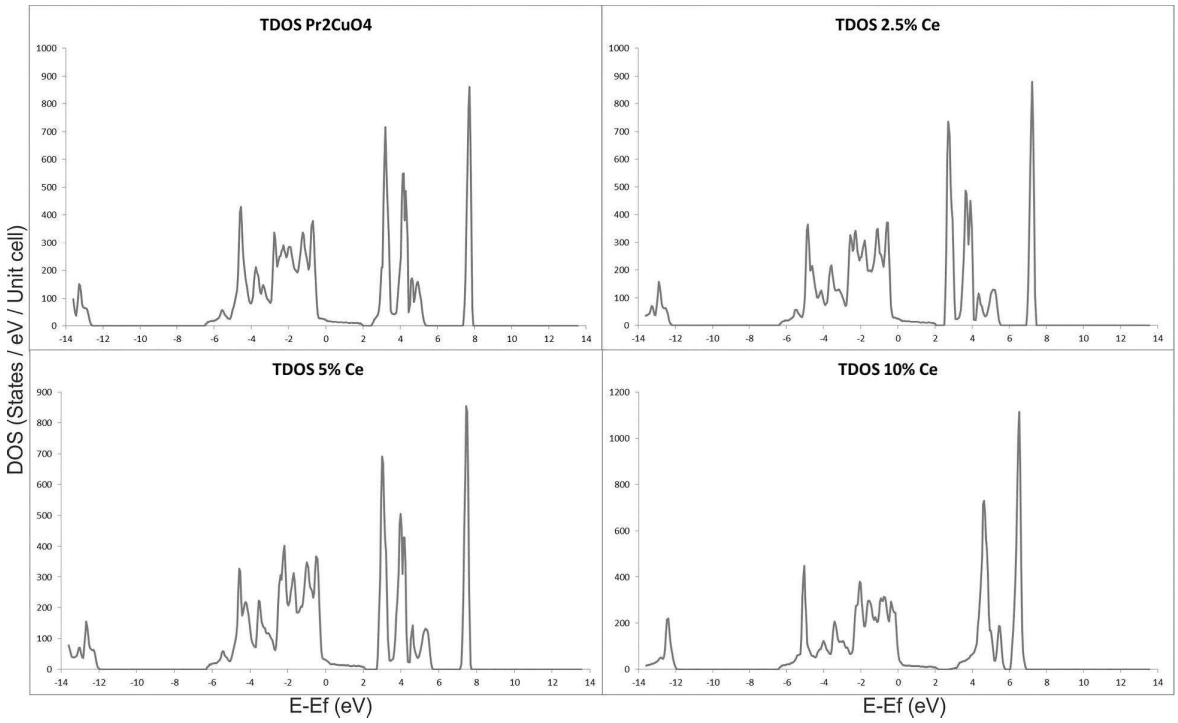


Fig. 4. Total densities of states (DOS) near the Fermi level for $Pr_2CuO_4$ (top left), $Pr_2CuO_4$ with 2.5% (top right), 5% (bottom left), and 10% (bottom right) Ce for Pr substitution. Fermi energy is at zero.

However, in our case we are more interested in the shifts of the DOS near the Fermi level upon substituting small amounts of Pr by Ce, therefore using an idealized structure and VCA should not prevent us from observing possible qualitative changes in electronic structure. 4*f*-orbitals do not contribute to the DOS in the direct vicinity of the Fermi level (Fig. SI3): they are located below -4 eV in the valence band and above 3 eV in the conduction band for the non-

substituted cuprate, and the gap between them only increases upon adding cerium atoms. This agrees with the results of the DFT/LSDA+*U* calculations on $PrBa_2Cu_4O_8$ and $Pr_2Ba_4Cu_7O_{15-y}$ [30] that show 4*f*-states below the Fermi level and no significant mixing between Pr and O states. However, the same authors observed strong Pr 4*f* and O 2*p* mixing on the Fermi level for $PrBa_2Cu_3O_7$, which once again emphasizes crucial importance of atomic environments for the properties of the compounds.

Our calculations show that, despite having no strong interactions with $CuO_2$ system, electronic structure of atoms in rare earth positions has visible impact on the general DOS picture. Upon an increase in the Ce content from 0 to 10 atomic %, the Fermi level in the model compounds moves towards the higher density of states. For 2.5% and 5% substituted cuprates it still resides in the flat area of the DOS, but at 10% it moves to the high density of states area formed by Cu 3*d* and O 2*p* states. Thus, on the quantitative level we do not see the dramatic change in the density of states for the sample with 2.5% Ce. However, we observe definite increase in both Cu 3*d* and O 2*p* partial DOS upon the increase in cerium content, therefore, the doping of $Pr_2CuO_4$ by cerium affects the electron density in the Cu-O system, which is an interesting effect and might be one of the factors partially responsible for the observed increase of electric conductivity for partially substituted praseodymium cuprates. However, electrical conductivity does not increase steadily with Ce content as was revealed by direct measurements. The presence of extra oxygen atoms likely affects the charge carrier concentration and might be a reason for the observed decrease of electric conductivity for heavily doped $Pr_{2-x}Ce_xCuO_4$.

***Electrochemical characterization of $Pr_{2-x}Ce_xCuO_4$ electrodes***

To gain some insight into the electrocatalytic activity of the $Pr_{2-x}Ce_xCuO_4$ in ORR, impedance measurements were carried out using the $Pr_{2-x}Ce_xCuO_4$|GDC|$Pr_{2-x}Ce_xCuO_4$ electrochemical cells. Typical impedance spectra recorded for $Pr_{2-x}Ce_xCuO_4$ (x = 0, 0.05 and 0.15) electrodes at 660°C in air and normalized by the electrode area are presented in Fig. 5 (a-c). To facilitate the comparison of ASR in the impedance plot, the spectra were corrected by the value of a high-frequency resistance (intercept) attributed to the ohmic resistance of the electrochemical cell, which is comparable with the electrolyte resistance.

The impedance spectra of the $Pr_2CuO_4$ and $Pr_{1.95}Ce_{0.05}CuO_4$ electrodes can be fitted using the equivalent electric circuit (EEC) consisting of two parts of a resistance and a constant phase element connected in series: ($R_1$-$CPE_1$)-($R_2$-$CPE_2$) (Fig. 5a and 5b). The ORR on the $Pr_2CuO_4$ electrode was comprehensively discussed in Ref. 18. In case of the heavily Ce-doped electrodes $Pr_{1.85}Ce_{0.15}CuO_4$ one may note a change in the shape of the spectrum (Fig. 5c): it can be presented as an overlap of three arcs and can be satisfactory fitted to the equivalent circuit with a

configuration of $(R_1\text{-}CPE_1)\text{-}(R_2\text{-}CPE_2)\text{-}(R_3\text{-}CPE_3)$. Every arc in an impedance spectrum implies a distinct rate-determining step of ORR process. The contribution into the overall electrode process of the high frequency arc, which is commonly associated with electron and ion transfer processes, increases with the Ce content. The presented results support a suggestion that rare-earth atoms may impact the ORR, though it is generally believed that transition metals mainly take part in oxygen reduction[43,44].

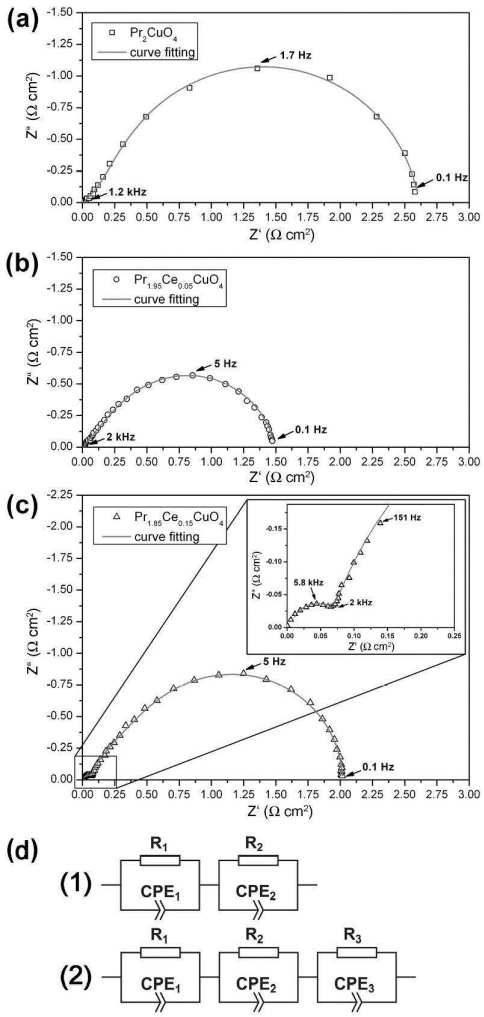


Fig. 5. Impedance spectra of the $Pr_{2-x}Ce_xCuO_4$ electrodes deposited on GDC electrolyte at 660°C in air: (a) – x = 0; (b) – x = 0.05; (c) – x = 0.15. (d) – equivalent electrical circuits used for fitting the impedance spectra: (1) – for (a) and (b), (2) – for (c).

The area specific resistance (ASR) was calculated as a difference between high- and low-frequency intercepts on a real axis after the correction by electrode area. The ASR values of $Pr_{2-x}Ce_xCuO_4$ as a function of temperature were plotted together in the Fig. 6.

As can be seen from Fig. 6, the ASR temperature dependencies are linear below and above 740 °C and have inflection near this point, which is commonly associated with a change in

the rate-determining step of the ORR[19]. Apparent activation energy ($E_a$) was calculated using the linear parts of the Arrhenius plot for logarithm of the inverse ASR value. It is worth to mention that no meaningful changes in $E_a$ is observed within the temperature range of 620-740 °C and $E_a$ is calculated to be 1.47±0.02 eV for all studied samples. As temperature rises up to 740-830 °C, $E_a$ drops down from 1.19 eV for x = 0 to 0.93 eV, 0.91 eV for x = 0.05 and 0.15, respectively. Enhancement of electrocatalytic activity of the cuprates in ORR by Ce-doping is reflected in the decrease in $E_a$. Lowering the $E_a$ results in a weaker ASR dependence upon temperature, therefore, some fluctuations in temperature during SOFC operation do not exert considerably on the cathode performance, which is favorable for a sustainable operation.

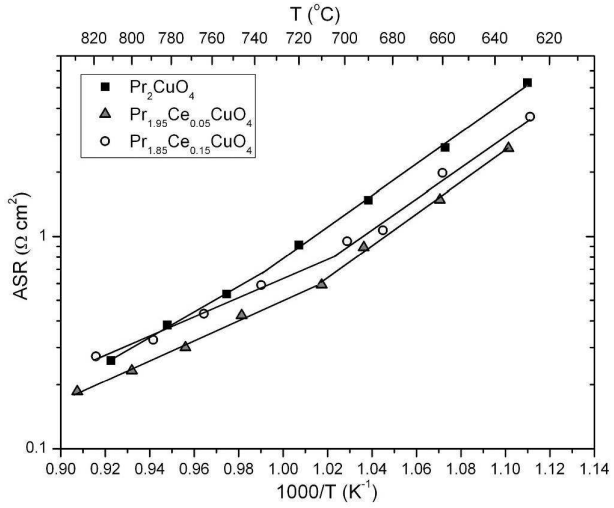


Fig. 6. ASR of $Pr_{2-x}Ce_xCuO_4$ (x = 0; 0.05; 0.15) as a function of temperature in air.

The lowest ASR among the considered cuprates was achieved for the $Pr_{1.95}Ce_{0.05}CuO_4$ composition (0.72, 0.39 and 0.23 $\Omega \cdot cm^2$ at 700, 750 and 800 °C, respectively) with the highest conductivity and retains under cooling/heating cycling for a week. Therefore, electrical conductivity is an influential factor for improving the electrode performance though it cannot be considered separately from the electrocatalytic activity. An increase in Ce content leads to higher ASR, however, the values are still lower in comparison to undoped $Pr_2CuO_4$ at lower temperature (T < 700 °C). It is worth mentioning that at higher temperature (T > 700 °C) the conductivity of $Pr_{1.85}Ce_{0.15}CuO_4$ is 3 times lower whereas ASR values practically coincide with those for $Pr_2CuO_4$. This fact is testifying in favor of even a small Ce doping is able to enhance the $Pr_2CuO_4$ electrocatalytic activity in ORR. The ASR of the $Pr_{1.95}Ce_{0.05}CuO_4$ electrode deposited on GDC solid electrolyte is 4 times lower than that of $La_{0.8}Sr_{0.2}MnO_3$ (LSM)[45] and 2 times lower than that of $La_{0.7}Sr_{0.25}FeO_3$ (LSF)[46] electrodes at 700 °C in air. Considering the data for other rare-earth (La, Pr, Nd) containing cathodes[38,47-49], it worth to note that ASR for the electrodes based on the screen-printed mixed oxides with the layered $K_2NiF_4$-type structure are

comparable with those achieved in the present work. The recent works aimed in ASR lowering revealed that significant progress have been observed in case of composite cathodes[20,50] or employing of an infiltration technique for the electrode formation[51,52].

***Performance of PCCO cathodes in an electrolyte-supported fuel cell***

In order to evaluate the $Pr_{2-x}Ce_xCuO_4$ cathode performance under conditions close to the real operation, the composition that exhibited the best characteristics during the primary tests was used as an oxygen reduction electrode in a fully assembled single fuel cell. The highest electrical conductivity, better mechanical compatibility with the GDC electrolyte, and lowest ASR among the studied $Pr_{2-x}Ce_xCuO_4$ oxides point to the x = 0.05 composition as a perspective cathode material. A fuel cell cross-section image made after electrochemical tests is shown in Fig. 7.

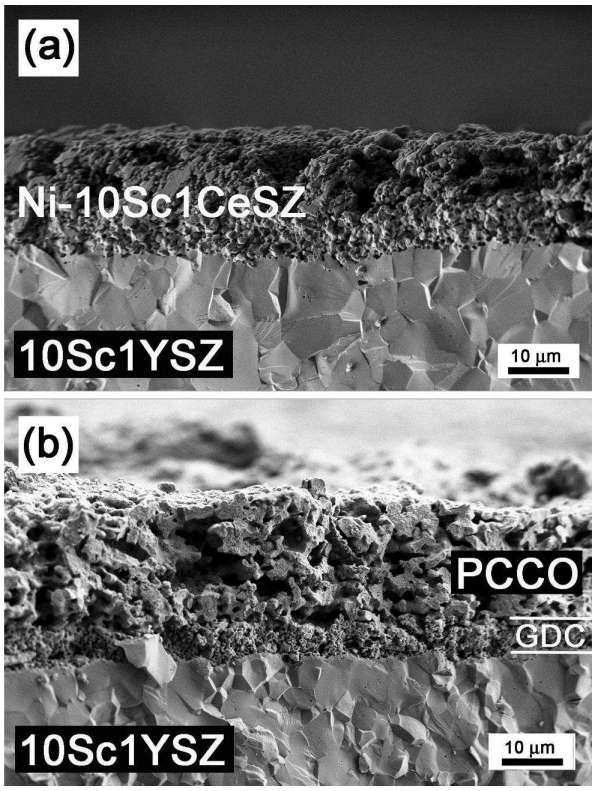


Fig. 7. A cross-section SEM image of the Ni-10Sc1CeSZ|10Sc1YSZ|GDC|PCCO fuel cell: Ni-10Sc1CeSZ|10Sc1YSZ (a) and PCCO|GDC|10Sc1YSZ (b) interfaces. Cross-sections were done after electrochemical measurements of the cell.

The 10Sc1YSZ electrolyte is dense without visible porous, having good bonding with the GDC interlayer. A $Pr_{1.95}Ce_{0.05}CuO_4$ cathode layer with a thickness of ~15 µm deposited on one

side of the electrolyte-supported cell is well adhered to the electrolyte substrate and demonstrates reasonable porosity.

The single fuel cell was tested in the operating temperature range of 700-900 °C with synthetic air as oxidant and humidified $H_2$ as fuel. The cell voltage and power density as a function of current density are plotted in Fig. 8a. The peak power densities generated by the cell were 308, 150, and 88 mW·cm$^{-2}$ at 900 °C, 800 °C, and 750 °C, respectively. To study the long-term stability of the single fuel cell with the $Pr_{1.95}Ce_{0.05}CuO_4$ cathode, the output power density at 800°C was measured under current density load of 150 mA·cm$^{-2}$ for 100 hours (Fig. 8b). The measurements show that the cell power density value was around 104 mW·cm$^{-2}$ during the long-term test.

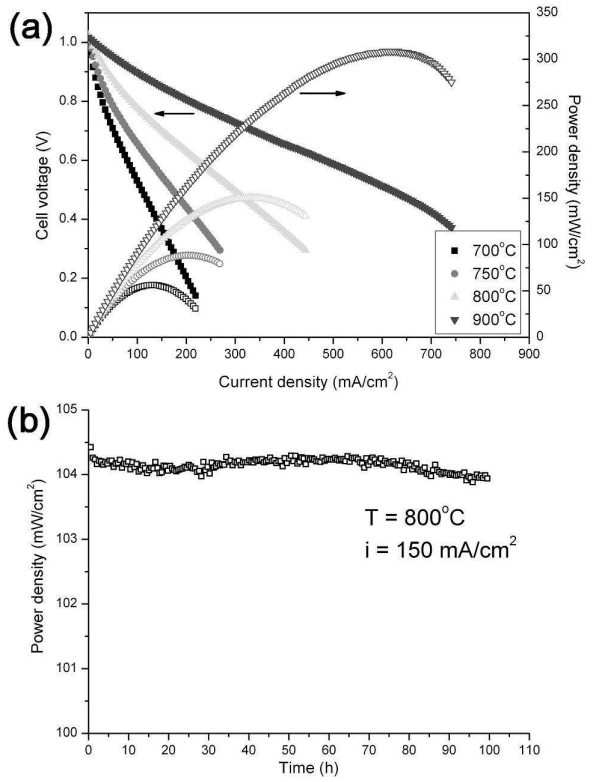


Fig. 8. The test of the electrolyte-supported fuel cell with the $Pr_{1.95}Ce_{0.05}CuO_4$ cathode: (a) – the current–voltage (filled points) and the corresponding power density (open points) curves; (b) – the output power density measured at 800°C under current density load of 150 mA/cm$^2$ as a function of time.

The presented electrolyte-supported cell performances exceed corresponding values for the undoped $Pr_2CuO_4$[53] and are comparable to those reported in[54,55] for $Pr_2NiO_4$ and $Sr_{0.7}Ce_{0.3}MnO_{3-\delta}$, respectively, measured using the analogues cell constructions. Although it is difficult to expect the encouraging performance in an electrolyte-supported cell, the observed

fuel cell performances are not limited, and it remains possible to improve them through further microstructural optimization and surface modification. It is worth noting that ASR of the cathode/electrolyte interface is 4 times lower at 700-900 °C as compared to ohmic losses mainly caused by electrolyte resistance (ASR ($Pr_{1.95}Ce_{0.05}CuO_4$) = 0.23 $\Omega \cdot cm^2$ and $R_{ohm}$(10Sc1YSZ) = 1.1 $\Omega \cdot cm^2$ (for the electrolyte thickness of 0.50 mm) at 800 °C in air[56]). Therefore, there are broad opportunities for a drastic performance enhancement of the cell with a new cathode material based on $Pr_{1.95}Ce_{0.05}CuO_4$ by employment of, for example, a thin film technology. Implementation of the $Pr_{2-x}Ce_xCuO_4$-GDC composite cathode material can improve the cell performance by elongation of a triple phase boundary and intensification of oxide-ion transport. Meanwhile, reducing the electrolyte thickness also should be conducive for enhancement of the fuel cell power density.

## Conclusion

The systematic investigation of novel Co-free cathode materials $Pr_{2-x}Ce_xCuO_4$ for SOFC application revealed the desired combination of physical and chemical characteristics. $Pr_{2-x}Ce_xCuO_4$ demonstrate electrical conductivity up to 120 $S \cdot cm^{-1}$ at 800 °C for the lightly doped sample with $x = 0.05$. Further increase in Ce-content above $x = 0.05$ leads to a gradual decrease in electrical conductivity. HT XRD analysis shows increase in thermal expansion coefficient from $11.9 \cdot 10^{-6}$ $K^{-1}$ (for x = 0) to $14.2 \cdot 10^{-6}$ $K^{-1}$ for x = 0.15, which is compatible with that for GDC solid electrolyte. Electrocatalytic activity studies using a symmetric cell with $Pr_{2-x}Ce_xCuO_4$ electrodes in ORR have shown that the *ASR* value of 0.39 $\Omega \cdot cm^2$ was achieved at 750 °C in air for the composition with the highest electrical conductivity. The peak power density generated in the test of a fully assembled single electrolyte-supported fuel cell with $Pr_{1.95}Ce_{0.05}CuO_4$ cathode is 150 $mW \cdot cm^{-2}$ at 800 °C. Therefore, small Ce-doping in $Pr_2CuO_4$ can substantially enhance its performance as a SOFCs cathode material. High electrical conductivity, chemical stability and mechanical compatibility with the electrolyte as well as good catalytic activity in ORR allow considering $Pr_{1.95}Ce_{0.05}CuO_4$ as a promising candidate for potential use as the SOFC cathode material.

## Acknowledgments

This work was partially supported by Russian Foundation for Basic Research (grant no. 15-38-20247), Skolkovo Institute of Science and Technology (Center of electrochemical energy), and MSU-development Program up to 2020. K.L.M. is grateful to Haldor Topsøe A/S for the financial support.

**Footnotes**

† Electronic Supplementary Information (ESI) available: X-ray diffraction and Thermogravimetric data. See DOI:

[a]Department of Chemistry, Moscow State University, Moscow 119991, Russia

[b]Institute of Problems of Chemical Physics RAS, Chernogolovka 142432, Russia

[c]Kurnakov Institute of General and Inorganic Chemistry RAS, Moscow 119991 Russia

[d]EMAT, University of Antwerp, Groenenborgenloan 171, B2020, Antwerp, Belgium

[e]Skoltech Center for Electrochemical Energy Storage, Skolkovo Institute of Science and Technology, 143026 Moscow, Russian Federation

[f]Institute of Solid State Physics RAS, Chernogolovka 142432, Russia

*Corresponding author: mazo@inorg.chem.msu.ru, Tel.: +74959395245, Fax: +74959390998

**References**

1. K. Sundmacher, *Ind. Eng. Chem. Res.*, 2010, **49**, 10159.
2. O. Z. Sharaf and M. F. Orhan, *Renew. Sust. Energy Rev.*, 2014, **32**, 810.
3. T. A. Adams, J. Nease, D. Tucker and P. I. Barton, *Ind. Eng. Chem. Res.*, 2013, **52**, 3089.
4. W. C. Junk and H. L. Tuller, *Adv. Energy Mater.*, 2011, **1**, 1184.
5. A. J. Jacobson, *Chem. Mater.*, 2010, **22**, 660.
6. J. G. Lee, J. H. Park and Y. S. Shul, *Nature Commun.*, 2014, **5**, 4045.
7. S. Choi, S. Yoo, J. Kim, S. Park, A. Jun, S. Sengodan, J. Kim, J. Shin, H. Y. Jeong, Y. Choi, G. Kim and M. Liu, *Sci. Rep.*, 2013, **3**, 2426.
8. N. Arulmozhi, W. H. Kan, V. Thangadurai and K. Karan, *J. Mater. Chem. A*, 2013, **1**, 15117.
9. A. Tarancon, M. Burriel, J. Santiso, S. J. Skinner and J. A. Kilner, *J. Mater. Chem.*, 2010, **20**, 3799.
10. J. E. H. Sansom, E. Kendrick, H. A. Rudge-Pickard, M. S. Islam, A. J. Wright, P. R. Slater, *J. Mater. Chem.*, 2005, **15**, 2321-2327.
11. A. P. Khandale and S. S. Bhoga, *J. Power Sources*, 2010, **195**, 7974.
12. M. Soorie and S. J. Skinner, *Solid State Ionics*, 2006, **177**, 2081.
13. H. Y. Hwang, S.-W. Cheong, A. S. Cooper, L. W. Rupp Jr and B. Batlogg, *Phys. C*, 1992, **192**, 362.
14. B. Raveau, *Angew. Chem. Int. Ed.*, 2013, **52**, 167.

15. M. S. Kaluzhskikh, S. M. Kazakov, G. N. Mazo, S. Ya. Istomin, E. V. Antipov, A. A. Gippius, Yu. Fedotov, S. I. Bredikhin, Yi Liu, G. Svensson and Z. Shen, *J. Solid State Chem.*, 2011, **184**, 698.
16. H. Hayashi, M. Kanoh, C.J. Quan, H. Inaba, S. Wang, M. Dokiya and H. Tagawa, *Solid State Ionics*, 2000, **132**, 227.
17. Q. Li, H. Zhao, L. Huo, L. Sun, X. Cheng and J. C. Grenier, *Electrochem. Commun.*, 2007, **9**, 1508.
18. G. N. Mazo, S. M. Kazakov, L. M. Kolchina, S. Ya. Istomin, E. V. Antipov, N. V. Lyskov, M. Z. Galin, L. S. Leonova, Yu. S. Fedotov, S. I. Bredikhin, Yi Liu, G. Svensson and Z. Shen, *Solid State Ionics*, 2014, **257**, 67.
19. N.V. Lyskov, M. S. Kaluzhskikh, L. S. Leonova, G. N. Mazo, S. Ya. Istomin and E. V. Antipov, *Int. J. Hydrogen Energy*, 2012, **37**, 18357.
20. L. M. Kolchina, N. V. Lyskov, D. I. Petukhov and G. N. Mazo, *J. Alloys Compd*., 2014, **605**, 89.
21. C. Sun, Q. Li, L. Sun, H. Zhao and L. Huo, *Mat. Res. Bull.*, 2014, **53**, 65.
22. C. A. Hancock, J. M. Porras-Vazquez, P. J. Keenan and P. R. Slater, *Dalton Trans.*, 2015, **44**, 10559.
23. Y. Tokura, H. Takagi and S. Uchida, *Nature*, 1989, **337**, 345.
24. N. P. Armitage, P. Fournier and R. L. Greene, *Rev. Mod. Phys.*, 2010, **82**, No. 3, 2421.
25. L.M. Kolchina, N.V. Lyskov, S.M. Kazakov, G.N. Mazo and E.V. Antipov, *RSC Adv.*, 2015, **5**, 91993.
26. ELK, an all-electron full-potential linearised augmented-plane wave (FP-LAPW) code, ver. 3.1.12. http://elk.sourceforge.net.
27. J. P. Perdew, A. Ruzsinszky, G. I. Csonka, O. A. Vydrov, G. E. Scuseria, L. A. Constantin, X. Zhou and K. Burke, *Phys. Rev. Lett.*, 2008, **100**, 136406.
28. V. I. Anisimov, I. V. Solovyev, M. A. Korotin, M. T. Czyzyk and G. A. Sawatzky, *Phys. Rev. B*, 1993, **48**, 16929.
29. A. G. Petukhov, I. I. Mazin, L. Chioncel and A. I. Lichtenstein, *Phys. Rev. B*, 2003, **67**, 153106.
30. A. Tavana, M. Shirazi and M. Akhavan, *Phys. Status Solidi B*, 2009, **246**, No. 10, 2287.
31. T. Kajitani, K. Hiraga, S. Hosoya, T. Fukuda, K. Oh-Ishi and Y. Syono, *Phys. C*, 1991, **178**, 397.
32. J. S. Higgins, Y. Dagan, M. C. Barr, B. D. Weaver and R. L. Greene, *Phys. Rev. B*, 2006, **73**, 104510.

33. J. Gauthier, S. Gagné, J. Renaud, M.-È. Gosselin and P. Fournier and P. Richard, *Phys. Rev. B*, 2007, **75**, 024424.
34. P. Richard, G. Riou, S. Jandl, M. Poirier, P. Fournier, V. Nekvasil and M. Divis, *Phys. C*, 2004, **408**, 830.
35. G. Riou, P. Richard, S. Jandl, M. Poirier, P. Fournier, V. Nekvasil, S. N. Barilo and L. A. Kurnevich, *Phys. Rev. B*, 2004, **69**, 024511.
36. Y. Krockenberger, H. Irie, O. Matsumoto, K. Yamagami, M. Mitsuhashi, A. Tsukada, M. Naito and H. Yamamoto, *Sci. Rep.*, 2013, **3**, 2235.
37. H. Gu, K.K. Fung and C.Q. Jin, *Phys. C*, 1994, **222**, 57.
38. J. A. Kilner and M. Burriel, *Annu. Rev. Mater. Res*., 2014, **44**, 365.
39. P. H. T. Ngamou and N. Bahlawane, *Chem. Mater*., 2010, **22**, 4158.
40. C. Weber, K. Haule and G. Kotliar, *Nature Physics*, 2010, **6**, 574.
41. P. W. Anderson, *Science*, 1987, **235**, No. 4793, 1196.
42. H. Das and T. Saha-Dasgupta, *Phys. Rev. B*, 2009, **79**, 134522.
43. Z. Wang, R. Peng, W. Zhang, X. Wu, C. Xia and Y. Lu, *J. Mater. Chem. A*, 2013, **1**, 12932.
44. L. Wang, R. Merkle, Y. A. Mastrikov, E. A. Kotomin and J. Maier, *J. Mater. Res.*, 2012, **27**, No. 15, 2000.
45. E. P. Murray and S. A. Barnett, *Solid State Ionics*, 2001, **143**, 265.
46. J.M. Ralph, C. Rossignol and R. Kumar, *J. Electrochem. Soc.*, 2003, **150**, A1518.
47. B. Philippeau, F. Mauvy, C. Mazataud, S. Fourcade and J. C. Grenier, *Solid State Ionics*, 2013, **249**, 17.
48. T. Nomura, S. Nishimoto, Y. Kameshima and M. Miyake, *J. Ceram. Soc. Jpn.*, 2012, **120**, 534.
49. Z. Gao, L. V. Mogni, E. C. Miller, J. G. Railsback and S. Barnett, *Energy Environ. Sci.*, 2016, DOI: 10.1039/C5EE03858H.
50. H. Li, Z. Cai, Q, Li, C. Sun and H. Zhao, *J. Alloys Compd.*, 2016, DOI: 10.1016/j.jallcom.2016.05.350.
51. D. Ding, X. Li, S.Y. Lai, K. Gerdes and M. Liu, *Energy Environ. Sci.*, 2014, **7**, 552.
52. C. Nicollet, A. Flura, V. Vibhu, A. Rougier, J. M. Bassat and J. C. Grenier, *J. Power Sources*, 2015, **294**, 473.
53. K. Zheng, A. Gorzkowska-Sobas and K. Swierczek, *Mater. Res. Bull.*, 2012, **47**, 4089.
54. C. Ferchaud, J. C. Grenier, Y. Zhang-Steenwinkel, M. M. A. van Tuel, F. P. F. van Berkel and J.-M. Bassat, *J. Power Sources*, 2011, **196**, 1872.

55. I. Kuritsyna, V. Sinitsyn, A. Melnikov, Yu. Fedotov, E. Tsipis, A. Viskup, S. Bredikhin and V. Kharton, *Solid State Ionics*, 2014, **262**, 349.
56. T. I. Politova and J. T. S. Irvine, *Solid State Ionics*, 2004, **168**, 153.